IOPscience iopscience.iop.org

Home Search Collections Journals About Contact us My IOPscience

In inhomogeneity and emission characteristics of InGaN

This article has been downloaded from IOPscience. Please scroll down to see the full text article.

2001 J. Phys.: Condens. Matter 13 6993

(http://iopscience.iop.org/0953-8984/13/32/308)

View the table of contents for this issue, or go to the journal homepage for more

Download details:
IP Address: 171.66.16.226
The article was downloaded on 16/05/2010 at 14:05

Please note that terms and conditions apply.

J. Phys.: Condens. Matter **13** (2001) 6993–7010 PII: S0953-8984(01)25842-1

In inhomogeneity and emission characteristics of InGaN

Yoichi Kawakami[1], Kunimichi Omae[1], Akio Kaneta[1], Koichi Okamoto[1], Yukio Narukawa[2], Takashi Mukai[2] and Shigeo Fujita[1]

[1] Department of Electronic Science and Engineering, Kyoto University, Kyoto 606-8501, Japan
[2] Nitride Semiconductor Research Laboratory, Nichia Corporation, 491 Oka, Kaminaka, Anan, Tokushima 774-8601, Japan

E-mail: kawakami@kuee.kyoto-u.ac.jp

Received 15 June 2001, in final form 15 June 2001
Published 26 July 2001
Online at stacks.iop.org/JPhysCM/13/6993

Abstract
Recombination dynamics of spontaneous and stimulated emissions have been assessed in InGaN-based light emitting diodes (LEDs) and laser diodes (LDs), by employing time-resolved photoluminescence and pump and probe spectroscopy. As for an $In_{0.02}Ga_{0.98}N$ ultraviolet LED, excitons are weakly localized by 15 meV at low temperature, but they become almost free at room temperature (RT). It was found that addition of a small amount of In results in the reduction of nonradiative recombination centres originating from point defects. The internal electric field does exist in InGaN active layers, and induces a large modification of excitonic transitions. However, it alone does not explain the feature of spontaneous emission observed in an $In_{0.3}Ga_{0.7}N$ blue LED such as an anomalous temperature dependence of peak energy, almost temperature independence of radiative lifetimes and mobility-edge type behaviour, indicating an important role of exciton localization. The lasing mechanism was investigated for $In_{0.1}Ga_{0.9}N$ near ultraviolet (390 nm), $In_{0.2}Ga_{0.8}N$ violet–blue (420 nm) and $In_{0.3}Ga_{0.7}N$ blue (440 nm) LDs. The optical gain was contributed from the nearly delocalized states (the lowest quantized levels (LQLs) within quantum wells) in the violet LD, while it was from highly localized levels with respect to the LQL by 250 meV for the violet–blue LD, and by 500 meV for the blue LD. It was found that the photo-generated carriers rapidly (less than 1 ps) transferred to the LQL, and then relaxed to the localized tail within the timescale of a few ps, giving rise to the optical gain. Such gain spectra were saturated and other bands appeared in the vicinity of the LQL under higher photo-excitation.

0953-8984/01/326993+18$30.00 © 2001 IOP Publishing Ltd Printed in the UK

1. Introduction

In recent years, there have been heated arguments concerning the emission mechanism in InGaN-based semiconductors [1]. Some group claim that the large Stokes-like shift between absorption and emission is because of the effect of exciton localization caused by inhomogeneous distribution of In in InGaN active layers [2–4]. In contrast, other groups report that it is just as a result of the quantum confined Stark effect (QCSE) induced by large internal electric fields whose origins are piezo and spontaneous electric effects [5]. Such a discrepancy is probably because of two factors. The first reason is that the macroscopic optical data such as photoluminescence and absorption do not provide enough information. The second one is that the degree of localization, as well as the contribution from internal electric fields differs between samples because of the difference in growth conditions, such as growth method, reactor, gas flow, pressure, substrate treatment, growth temperature, mean In mole fraction, background impurities and so on. If the In composition is randomly distributed, and if the well barrier interface is atomically flat, the effect of localization will be very small. If the background carrier density is high in InGaN active layers, the internal electric field is screened to some extent depending on the carrier density. Similar effects also take place in the case of high photo-excitation. It is interesting to note that almost all InGaN well thicknesses in light emitting devices are as small as 2 to 3 nm. This is because it is essential for sufficient oscillator strength of excitons to achieve the overlapping of wavefunctions of a confined electron–hole pair forming exciton. In order to reach a general understanding of the emission mechanism, it would be important to accumulate a lot of reliable data reported by various groups.

In this paper, spatial inhomogeneity of optical properties and localization behaviour of excitons are generally surveyed. Then, recombination dynamics of spontaneous and stimulated emissions are assessed in InGaN-based light emitting devices, the emission energies of which range from 363 to 550 nm for LEDs, and from 390 to 440 nm for LDs by employing time resolved photoluminescence (TRPL) and pump and probe (P&P) spectroscopy.

2. General survey of localization behaviour of excitons

2.1. Macroscopic optical properties

As mentioned before, one has to be very careful in ascribing a Stokes-like shift or blue-shift of emission energy with increasing photo-excitation intensity solely to the effect of exciton localization. This is because large internal electric fields modify the absorption edge of InGaN quantum wells by the so-called quantum confined Franz–Keldysh effect (QCFK) and quantum confined Stark effect (QCSE) [5]. It has been reported that the Si doping in the GaN barriers results in the reduction of the Stokes-like shift and in the decrease of radiative recombination lifetime [6]. This is probably due, at least in part, to the screening of the internal electric field induced by the redistribution of doped electrons, besides the increase in structural and interface quality with increasing Si doping. However, there exist phenomena even in macroscopic optical spectroscopy that can not be interpreted by such QCFK and/or QCSE effects. They are, for example, (1) anomalous temperature dependence of emission peak energies, (2) almost temperature independence of radiative recombination lifetimes and (3) mobility edge behaviour.

2.1.1. Anomalous temperature dependence of emission peak energies. Generally, bandgap energies of semiconductors decrease with increasing temperature, namely, $E_0(T) = E_0 - \alpha T^2/(T + \beta)$, where α and β are known as Varshini's fitting parameters. For wurtzite GaN,

it has been reported that $\alpha = 0.375$ meV and $\beta = 270$ K for the temperature variation of A-exciton transition. This shows that the temperature induced red-shift of transition energies is about 60 meV between 0 K and 300 K. However, anomalous temperature dependence has been observed in InGaN active layers, where luminescence peak energies make a blue shift with respect to the values predicted by the Varshini formula. Eliseev *et al* [7] reported that such blue shifting behaviour can be interpreted by the effect of localized tail states assuming that the density of state (DOS) of excitons induced by potential fluctuation is of Gaussian form having dispersions of σ^2. In such a case, the luminescence peak $E_L(T)$ has an additional positive term as shown below.

$$E_L(T) = E_{L0} - \frac{\alpha T^2}{T + \beta} + \frac{\sigma^2}{k_B T^2}. \tag{1}$$

The term of σ shows the energy representing the degree of localization. The value of σ scatters in a wide range depending on the literature [8]. This suggests that the localization strongly depends on the growth conditions of InGaN active layers.

2.1.2. Temperature dependence of radiative recombination lifetimes. Besides the potential fluctuation, it is very important to know the spatial extent of localization centres in the plane of quantum wells (dimensionality in other words) that is an important factor for naming the system such as compositional fluctuation with micron scale, quantum disc, mesoscopic dot or quantum dot (QD). The temperature dependence of radiative lifetimes is an effective tool for the evaluation of dimensionality despite the macroscopic characterization. This is because the DOS of excitons in K (momentum) space is determined by the dimensionality [9], and the temperature dependence of exciton-oscillator strength is estimated by counting the number of excitons which satisfy the momentum conservation law. In the actual QWs, the depth and the spatial dimension of localization centres differ according to the structures. In the case of weak localization, excitons are easily thermalized to higher sub-bands within localization centres due to the small energy difference between the lowest quantized-level and upper sub-bands. In this case, radiative lifetime increases with temperature because the oscillator strength is averaged by the contribution from other upper transitions. If temperature is increased further, excitons may be delocalized to extended states with 2D DOS. In such a case, radiative lifetime increases in proportion to temperature [10]. If the degree of localization is large enough, the temperature dependence of the radiative lifetime becomes less dominant. It has been theoretically shown that the radiative lifetimes are almost independent of temperature up to room temperature if the excitons are confined in localization centres whose size is less than 3 nm [11].

2.1.3. Mobility edge behaviour. 'Mobility edge'-type behaviour has been observed in InGaN QWs in both spontaneous and stimulated emission, where the luminescence peak is insensitive to photo-excitation energy (E_{exc}) for energies higher than a certain energy (E_m), but as E_{exc} is tuned below E_m, the peak position makes a redshift quickly [12, 13]. Such phenomena can be interpreted by an energy relaxation for localized excitons. Once excitons are photo-generated, they relax quickly into localized states where further relaxation and spatial migration are possible only through the tunnelling between localized states. The relaxation rate for such a process strongly depends on the density of available final states with lower energy, and can be enhanced if the photo-excitation is made below the mobility edge.

2.2. *Spatial inhomogeneity of luminescence*

Chichibu *et al* [14] performed the cathodoluminescence (CL) spectrum mapping of $In_{0.1}Ga_{0.9}N$ single quantum wells (SQWs), and found that the broad CL band taken from a wide area consists of several sharp emission peaks having different peak energies. Moreover, monochromatic CL images showed that the emission area is spatially distributed with size less than 60 nm, whose resolution is limited by the diffusion length of the carriers (or excitons). Zhang *et al* [15] reported that a time-resolved CL study shows that carriers generated by electron-beam excitation will diffuse toward and recombine at neighbouring InN-rich centres, resulting in a strong lateral excitonic localization prior to radiative recombination. Scanning near-field optical microscopy (SNOM) is another effective tool to investigate the PL mapping. Vertikov *et al* [16] performed the SNOM-PL mapping in thin InGaN/GaN epilayers and QWs with the spatial resolution of 100 nm. Most of the SNOM results were obtained using a home-built illumination-mode system, where the laser light was focused into a few hundred nm^2 spot through the SNOM tip composed of a tapered optical fibre and the photoluminescence (PL) spectra were probed by objective lens. A drawback of such a system is that it is very difficult to know whether excitons and/or carriers producing PL are directly photo-generated at the probe region or are diffused from outside. This problem may be overcome by means of an illumination-collection mode developed recently for the assessment of widegap semiconductors, where photo-excitation and the PL probing are performed using the same fibre tip [17].

2.3. *Origin of localization centre*

It has been reported that the self-formation of an In-rich region may be the intrinsic nature of InGaN ternary alloys since the large difference in interatomic spacing between GaN and InN was found to give rise to a solid phase miscibility gap [18, 19]. Actually, cross-sectional transmission electron microscopy (TEM) and energy-dispersive x-ray microanalysis (EDX) revealed that the contrast of light and shade in the well layers observed in a TEM image corresponds to the difference in In compositions [2]. Since the In-rich region consists of an almost isotropic dot structure whose diameter is 3 nm on average, it acts as a QD at which excitons and/or carriers are deeply localized. Kisielowski *et al* [20] observed local compositional fluctuation with estimated diameters of 1–2 nm in the lattice images of a $GaN/In_{0.43}Ga_{0.57}N/Al_{0.1}Ga_{0.9}N$ QW structure obtained by high resolution TEM. After that, they did a systematic assessment for $In_xGa_{1-x}N$ samples with wider indium concentration and well thickness [21]. They reported that a piezoelectric-field based mechanism is shown to dominate in samples with thick wells ($L > 3$ nm) of low indium concentration ($x < 0.15$–0.20), while spatial indium-concentration fluctuations dominate luminescence properties in samples of higher indium concentration in thinner wells. It should be noted that some groups claim that the origin of localization is not In-rich InGaN alloys but nearly pure InN QDs [22, 23].

Some groups claim that the localization behaviour is not due to In-rich clustering but may be interpreted by the peculiar band structure of InGaN ternary alloys. Yamaguchi and Junnarkar [24] reported that an antibonding s-like state produced by the nitrogen vacancy (V_N) is predicted to appear at 0.3 eV below the conduction-band (CB) edge for GaN, which gets shallower and then resonant with the CB for $In_xGa_{1-x}N$. Therefore, the V_N was proposed as a candidate for the strong localization of excitons in $In_xGa_{1-x}N$. On the other hand, Bellaiche *et al* [25] reported that alloying of GaN with In induces localization in the hole wavefunction, resonating with the valence band even with perfectly homogeneous In distribution by means of

large supercell empirical pseudopotential calculations. Another model for the localization-like behaviour is that a polaron state of electrons contributes to the recombination process [26].

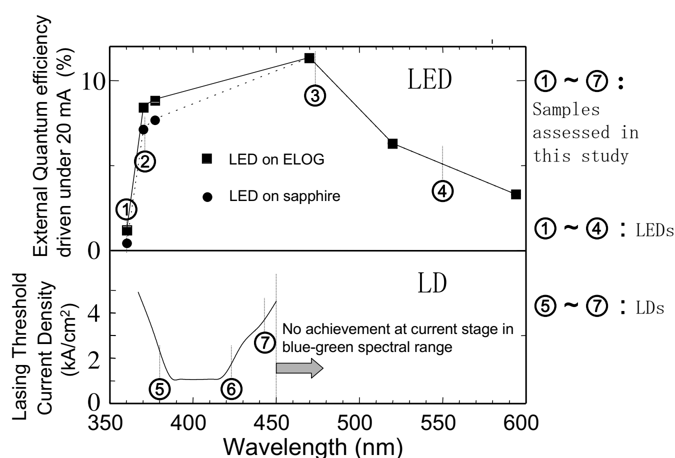

Figure 1. Current status of InGaN-based light emitting devices. External quantum efficiency driven under 20 mA is plotted for LEDs, and lasing current density reported so far is drawn for LDs.

3. Current status of InGaN-based light emitting devices

Current developments in the growth technology have led to the commercialization of dazzling blue, green and amber light emitting diodes (LEDs) [27, 28] and violet laser diodes (LDs) [29, 30], both of which are composed of InGaN/GaN/AlGaN-based hetero-structures. Figure 1 shows the performance of InGaN-based LEDs and LDs plotted as a function of emission wavelength. For LEDs, the external quantum efficiencies are plotted [31], and for LDs, the lowest lasing thresholds reported so far are shown. The external quantum efficiency of UV-LEDs using GaN as active layers is low, of the order of 1%. It can be doubled if the devices are grown by the epitaxial lateral over growth (ELOG) technique, where macroscopic dislocation density is reduced by three orders of magnitude compared to the layers grown directly on sapphire. Another interesting feature is that the addition of a small amount of In to the active layer results in the dramatic increase of the efficiency. Now, the maximum efficiency is achieved at 470 nm, which corresponds to a pure-blue colour. Efficiency just more than 10% is now commercially available, but further improvement is desired to extend the application area of LEDs, for example, for the lighting application. It should be improved up to 30 to 40% if the pathway to nonradiative recombination is completely eliminated. For blue LEDs, no difference is observed in the efficiency between ELOG and sapphire samples [32]. The efficiency is reduced if In mole fraction is increased further suggesting the re-activation of nonradiative centres, and the achievement of red colour emission with sufficient efficiency is still a challenging target. As for the performance of LDs, the tendency is different from that of LEDs. The lowest lasing threshold is achieved at 400 nm spectral range, that is 390 to 410 nm; however it goes up out of this range. The longest lasing wavelength under CW operation is 450 nm [33]; however the threshold current density was more than 4 kA cm^{-2}, and no achievement is reported so far for stable CW operation in the blue–green spectral range. This difficulty may be for two reasons. The first reason is due to the potential fluctuation induced by exciton localization [1–4, 9–12, 34]. It causes the inhomogeneous broadening of density

of states (DOS), so that the optical gain may not be sufficiently generated from such states. Another possibility is the internal electric field, which is enhanced with increasing compressive strain in InGaN layers [5]. Such an electric field may modify the DOS, and oscillator strength of excitons is suppressed [35]. Further breakthrough is therefore required to extend the application area of LEDs and LDs. Such targets can be facilitated by clearly understanding the emission mechanism, and by making positive feedback to the growth conditions and device structures.

4. Experimental procedure

Sample structures investigated in this study are summarized in table 1. It has to be noted that the In mole fractions are overestimated because they are not experimentally characterized data but just estimated according to the growth conditions. They probably have to be multiplied by 0.6 or 0.7 to get the exact values. The layer thickness of InGaN active layers is as small as 3 nm apart from ultraviolet (UV) LEDs.

Table 1. Sample structures of InGaN-based light emitting devices.

	In mole fraction (%)	Active layer (nm)	Number	Emission (nm)
UV LED-1	0	40 nm	1	363
UV LED-2	2	40 nm	1	369
Near-UV LD	10	3 nm	3	390
Violet–blue LED	20	3 nm	7	422
Blue LED	30	3 nm	1	471
Blue LD	30	3 nm	6	440
Yellowish green LED	35	3 nm	1	550

Pulsed photo-excitation for the TRPL of spontaneous emissions is provided by the frequency doubled (2ω) or frequency tripled (3ω) beams of a mode-locked Al_2O_3:Ti laser (ω) which was pumped by an Ar^+ laser. It is possible to make a selective excitation to $In_xGa_{1-x}N$ active layers by using a frequency doubled beam whose tuning range is from 350 to 530 nm. The pulse width used was 1.5 ps. The repetition rate of the laser is 80 MHz, and the time-interval is 12.5 ns. It can be reduced to 4 MHz by an acoustic optic (AO) modulator in order to avoid the multi-excitation depending on the decay times. The detection is performed by means of a fast scan streak camera in conjunction with monochromator using gratings whose grooves are 100, 300 and 1200 lines mm^{-1}. The time-resolution for the detection is about 2 ps.

Photo-pumped stimulated emissions were performed using a frequency dually doubled ($4\omega_S$) beam of an optical parametric amplifier which was pumped by a regenerative amplifier, the wavelength, pulse width and repetition rate of which was 390 nm, 150 fs and 1 kHz, respectively.

The P&P spectroscopy was performed for the measurement of temporal behaviour of differential absorption using a dual photo-diode array in conjunction with 25 cm monochromator [36]. The white light used for the probe beam was generated by focusing the part of the output beam from the regenerative amplifier on a D_2O cell. The delay time of the probe beam with respect to the pump beam was tuned by changing the position of the retroreflector, which could be controlled by the pulse stage. In order to detect the probe beam with spatially uniform carrier distribution in the sample, the focus size of the pump beam (600 μm in diameter) was set so as to be much larger than that of the probe beam (200 μm in diameter). Furthermore, the probe beam was perpendicularly polarized with respect to the pump beam, and the transmitted probe beam polarized in this direction was detected to avoid

the scattered component of the pump beam. The time origin depending on the photon energy was calibrated by the data of the optical Kerr effect of Al_2O_3.

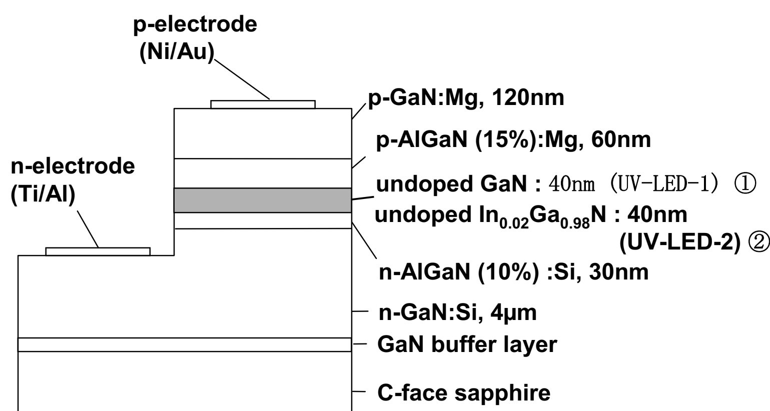

Figure 2. Schematic structure of UV LEDs, the active layers of which are composed of 40 nm undoped GaN for UV LED-1, and of 40 nm undoped $In_{0.02}Ga_{0.98}N$ for UV LED-2.

5. Results and discussion

5.1. Radiative and nonradiative recombination processes in LED structures

The device structures of UV LED-1 and UV LED-2 are shown in figure 2 [37]. The structural difference between the two is just the active layers, where GaN is used for UV LED-1 while a small amount of In, 2%, is incorporated into GaN ($In_{0.02}Ga_{0.98}N$) for UV LED-2. However, the external quantum efficiency is very different. It is about 1.5% for UV LED-1, and is about 6% for UV LED-2. Since the layer thickness of n-AlGaN layer is thin, layers are almost coherently grown on the n-GaN layer. An important point to make efficient UV LEDs is that the top contact layer thickness of p-GaN:Mg must be substantially small in order to reduce the self-absorption of electroluminescence (EL).

EL and absorption spectra of UV LED-2 taken at 20 K and room temperature (RT) are shown in figure 3(a). The absorption property was characterized by measuring photo-induced voltage (PV) and electroreflectance (ER) spectroscopy. Although the Stokes shift between EL and absorption spectra is about 15 meV at 20 K, no Stokes shift is observed at RT, indicating that the EL is contributed from free excitons. As depicted in figure 3(b) the EL peak energy of UV LED-2 is plotted as a function of temperature. For comparison, the dependence taken for a blue LED is also shown. As for UV LED-2, the peak energy slightly increases between 20 K and 70 K, and then decreases according to the T-dependence of the bandgap energy. This indicates that excitons are trapped at small potential minima at low temperature, and are delocalized above 70 K. However, the T-dependence of the blue LED is totally different from that of UV-LED-2. It gradually increases with temperature up to 300 K. This result suggests that exciton localization plays an important role for this sample even at RT. Radiative and nonradiative recombination times were characterized by means of TRPL spectroscopy. In order to estimate the internal quantum efficiency, selective excitation to an InGaN active layer was made by tuning the excitation photon energy. The radiative lifetime represents the oscillator strength of excitons. For $In_{0.02}Ga_{0.98}N$-UV LED-2, it is 230 ps at 20 K, and increases with temperature with T to the 1.5th dependence above about 50 K as shown in figure 4. Such dependence is

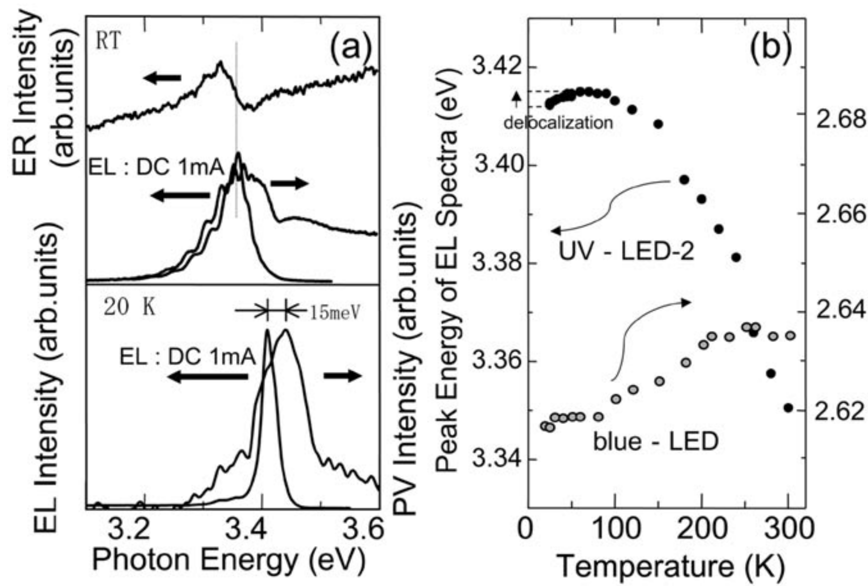

Figure 3. (a) The EL, PV and ER spectra at 20 K and at RT in UV LED-2 ($In_{0.02}Ga_{0.98}N$ active layer). (b) The temperature dependence of the EL peak energy for the UV LED-2, and for the blue LED.

same as that of GaN UV LED-1. This means that the oscillator strength of excitons decreases with temperature. The reason is that excitons with higher momentum generated by thermal population cannot recombine radiatively because the momentum conservation law with photon cannot be satisfied. Since the thermal population of the exciton's momentum changes with the DOS of excitons, the T-dependence of the radiative lifetime gives us information on the dimensionality of excitons [38–40]. In the case of T to the 1.5th dependence, excitons should be in three-dimensional (3D) states, T-linear dependence shows a two-dimensional (2D) feature and a zero-dimensional (0D) feature is suggested if radiative lifetimes have no temperature dependence. In this case, we have 1.5th dependence, so the result shows the 3D feature of excitons. This is consistent with the fact that the thickness of the active layer is as large as 40 nm. As can be seen in figure 4, the PL lifetime is mainly limited by the nonradiative recombination times at RT. The difference between GaN and $In_{0.02}Ga_{0.98}N$ is this nonradiative process. The nonradiative lifetime of $In_{0.02}Ga_{0.98}N$ is much larger than that of GaN, and is almost independent of temperature, indicating that the nonradiative recombination centres induced by some sort of point defect are greatly suppressed by the addition of a small amount of In to the layer [41].

Figure 5(a) shows the EL spectra and EL decay times plotted as a function of emission energies of the blue LED. At 20 K, the main emission band and its LO-phonon replica are observed. The EL lifetime is about 3 ns. At RT, the EL spectrum becomes broader at RT. One important feature is that the EL peak is blue-shifted compared with the spectrum at 20 K. As mentioned before, this is not consistent with the T-dependence of bandgap energy. EL, radiative and nonradiative lifetimes are plotted as a function of temperature in figure 5(b). The radiative lifetime slightly changes from 3.3 ns to 4.4 ns when the temperature is increased from 20 K to 300 K. So, almost no temperature independence of radiative lifetimes was observed in this sample, suggesting the zero-dimensional feature of excitons. Actually, theoretical

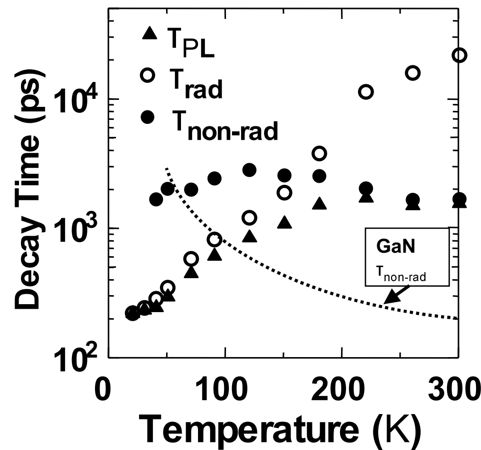

Figure 4. The temperature dependence of τ_{PL}, τ_{rad} and τ_{nonrad} in UV LED-2 ($In_{0.02}Ga_{0.98}N$ active layer). The data of τ_{nonrad} in a GaN layer are drawn for comparison.

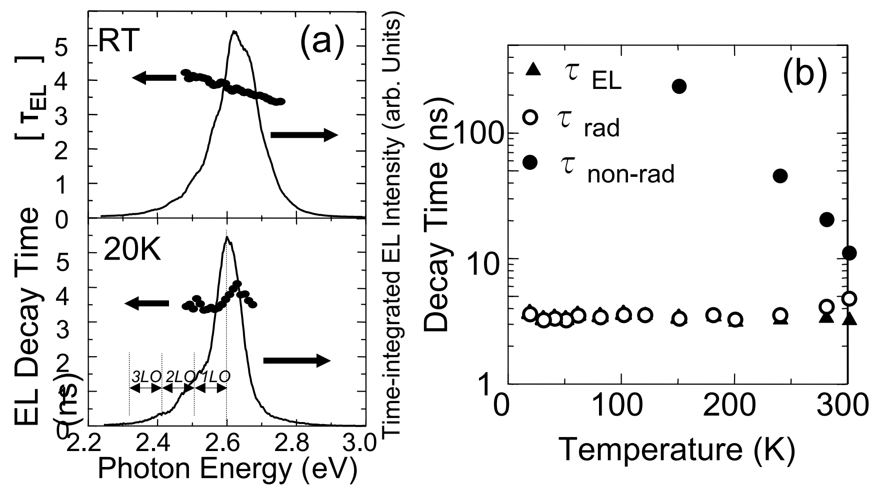

Figure 5. (a) Time-integrated EL spectra and EL lifetimes as a function of emission energy at 20 K and at RT obtained for the blue LED. (b) Temperature dependence of τ_{EL}, τ_{rad} and $\tau_{non-rad}$ in the blue LED.

calculation predicts that the spatial extent of the localization centre should be in the order of 3 nm to account for such a T-dependence [11]. In this particular sample, at RT, the external quantum efficiency is more than 20% if driven at 1 mA, and the internal quantum efficiency is estimated to be about 60%, which is substantially large. It is likely that such high efficiency is contributed from the zero-dimensional feature because capture cross-sections to nonradiative recombination centres are greatly suppressed once excitons are trapped at deep localization centres [3]. In order to grasp every experimental result, a feasible model of the exciton dynamics in the InGaN blue LED is schematically illustrated in figure 6. That is, excitons are deeply localized, but each site is closely distributed and/or each site is energetically connected. Therefore, the tunnelling or phonon-assisted hopping to higher energy sites is possible at elevated temperature.

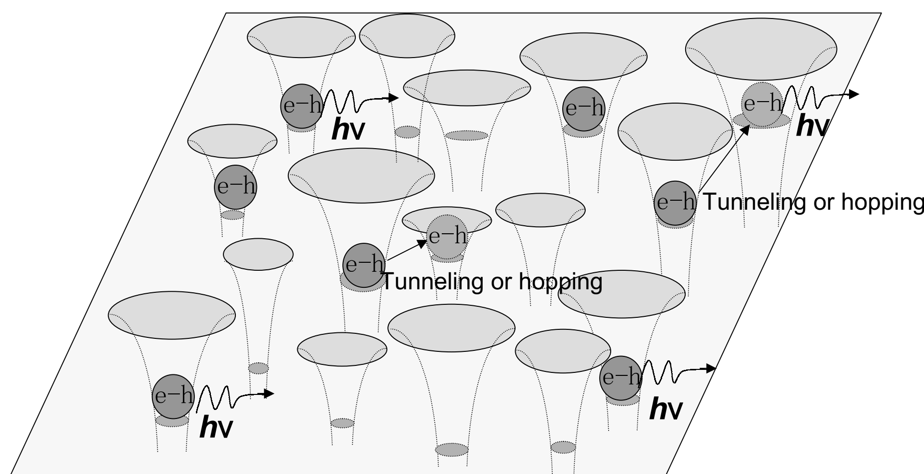

Figure 6. A feasible model for the dynamics of localized excitons in the blue LED.

The normal optical spectroscopy is macroscopic characterization. It is important to develop the technique having spatial resolution in order to make clearer correlation between microscopic or nanoscopic structures and optical properties. We have already set up a TRPL spectroscopy having 1 μm spatial resolution by using a UV optical microscope [42, 43]. However, spatial resolution has to be improved to get more detailed data. We have recently performed the PL imaging of an InGaN-based single quantum well (SQW) using scanning near-field optical microscopy (SNOM) under illumination–collection mode, where photo-excitation and the PL probing are performed using the same fibre tip. This was achieved by tailoring the tapered structure of the fibre tip composed of a pure SiO_2 core to transmit UV light with low transmission loss, and to eliminate the emission background from the fibre [17]. Figure 7 shows preliminary data taken for an InGaN SQW based yellowish-green LED structure at RT. Figure 7(a) is the image mapped with the PL peak wavelength, where a fluctuation from 535 nm to 550 nm is observed with the minimum size of about 0.1 μm. Figure 7(b) is the one mapped with the PL peak intensity. The PL intensity is fluctuated from the level of 0.8 to 1.8. Clear correlation between the PL peak and intensity has not been observed in this condition. The macroscopic optical measurement shows that internal quantum efficiency of this layer is about 20%; however this picture shows that such values fluctuate from 10% to 50% depending on the location. The TRPL spectroscopy using this SNOM equipment at various temperatures is in progress.

5.2. Recombination dynamics of dense carriers in LD structures

Figure 8 shows sample structures of (a) near-UV, (b) violet–blue and (c) blue LDs. The whole samples consist of the separate confinement heterostructure where (a) the Si-doped $In_{0.1}Ga_{0.9}N$ (3 nm)/$In_{0.02}Ga_{0.98}N$ (6 nm) multiple quantum well (MQW) with three periods, (b) the undoped $In_{0.2}Ga_{0.8}N$ (3 nm)/$In_{0.05}Ga_{0.95}N$ (6 nm) MQW with seven periods or (c) the undoped $In_{0.3}Ga_{0.7}N$ (3 nm)/$In_{0.05}Ga_{0.95}N$ (10 nm) MQW with six periods is sandwiched between GaN waveguide layers (0.1 μm in each) and (a) $Al_{0.15}Ga_{0.85}N$, (b) $Al_{0.07}Ga_{0.93}N$, (c) $Al_{0.15}Ga_{0.85}N$ cladding layers (0.4 μm in each). The top of the $Al_xGa_{1-x}N$ clad and the GaN waveguide are Mg-doped p-type layers, while the bottom of the clad and the waveguide are Si-doped n-type layers. The LD operation at RT was performed at 390 nm under CW mode

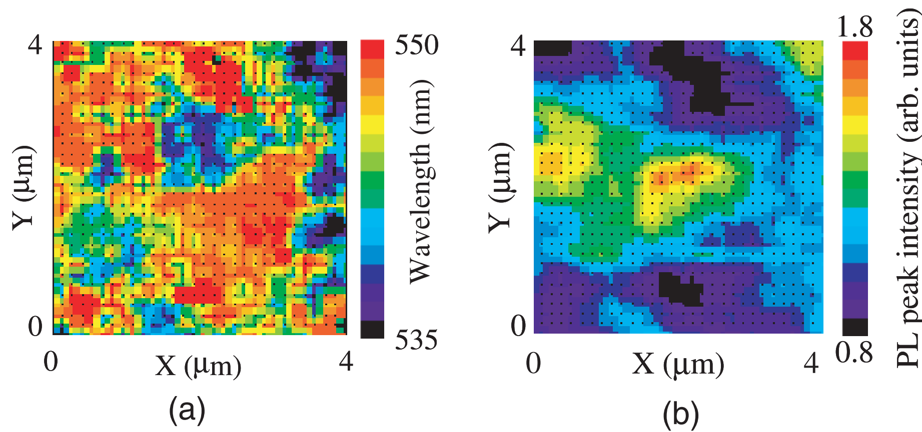

Figure 7. Near-field PL images taken for a yellowish-green LED structure mapped with (a) the PL peak wavelength, and with (b) PL-peak intensity.

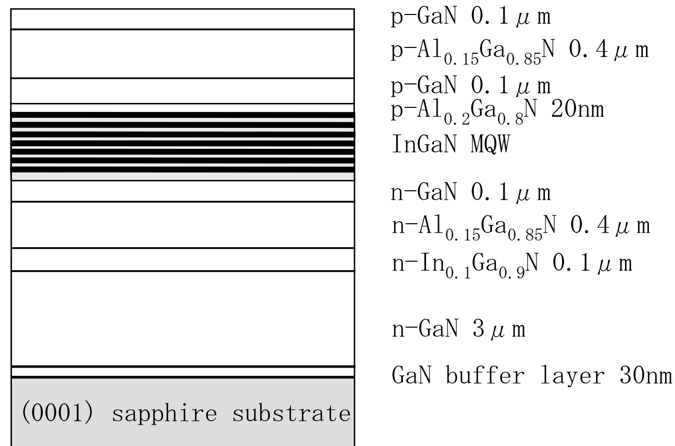

Figure 8. Schematic diagram of device structures of (a) near-UV LD, (b) violet–blue LD and (c) blue LD.

for sample a, at 420 nm under pulsed mode for sample b and at 440 nm under pulsed mode for sample c.

Figure 9 shows time-integrated photoluminescence (TI-PL) spectra under photo-excitation energy density (I_{ex}) of 100 nJ cm^{-2} taken for three types of LD. Absorption (OD) spectra under low photo-excitation (Xe lamp) corresponding to DOS are also depicted in the figure. The lowest quantized energy levels within the wells (designated as E_{ex1hh}) were estimated by ER spectroscopy. In contrast to sample a, the PL spectra for samples b and c are composed of two emission bands, and the main bands are located on the low energy side with respect to E_{ex1hh} by 250 meV and 500 meV, respectively. The blue-shift of these bands under increased I_{ex} conditions (from 10 nJ cm^{-2} to 20 μJ cm^{-2}) is about a few tens of meV, which is substantially smaller that the energy difference between two emission bands. These phenomena were attributed to the localization of excitons whose origin is probably due to In-rich quantum dot (QD)-like centres. This model is supported by the EDX microanalysis using scanning

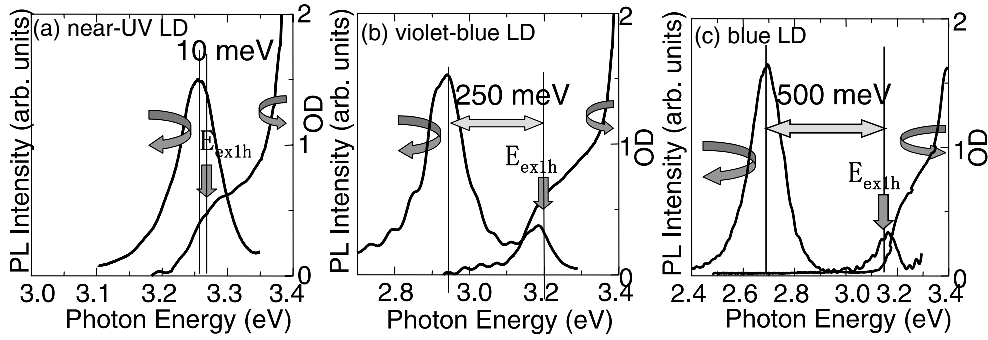

Figure 9. TI-PL and optical density (OD) spectra taken for (a) near-UV LD, (b) violet–blue LD and (c) blue LD.

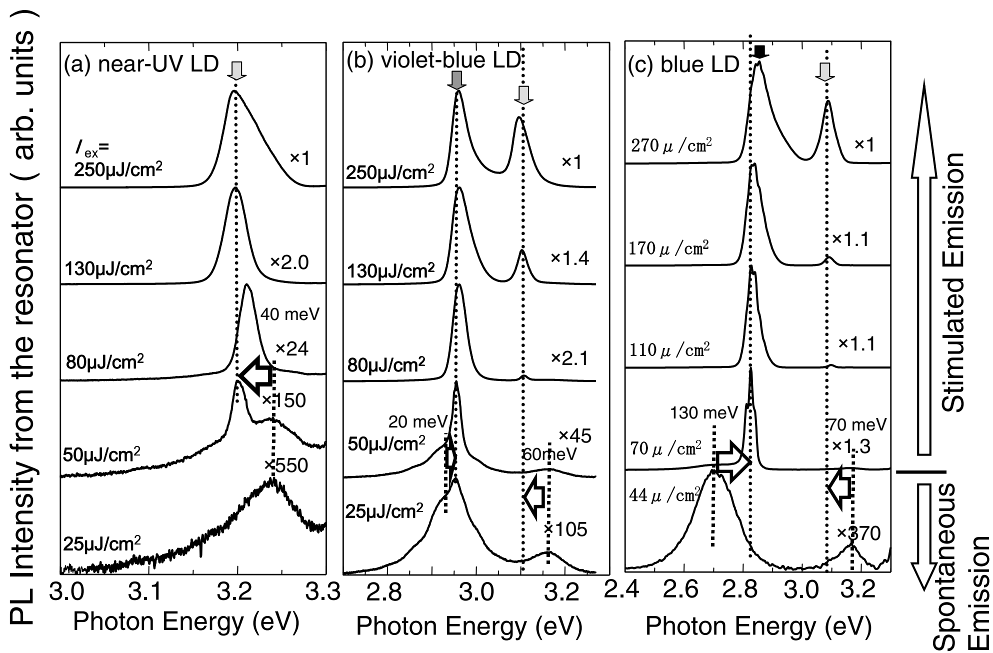

Figure 10. Time-integrated PL from the resonator under various excitation energy densities taken at (a) near-UV LD, (b) violet–blue LD and (c) blue LD.

transmission electron microscopy (STEM) [11]. Moreover, the zero-dimensional feature of excitons was revealed for temperature dependence of radiative lifetimes in samples b and c.

The TI-PL spectra were detected with the edge geometry from the resonator, the cavity length of which was about 1 mm. As shown in figure 10, stimulated emission (SE) was observed from every sample if I_{ex} was more than about 50 μJ cm^{-2}. SE appeared on the low energy side of the spontaneous emission (SPE) for the sample a. The energy difference between SE and SPE peaks is about 40 meV. This is probably because of the effect of bandgap renormalization. However, blue-shifts were observed by 20 meV for sample b, and by 130 meV for sample c, respectively. The band filling and/or photo-induced screening of internal electric fields result in blue-shift, and such effects probably play a more important role for localized states in samples b

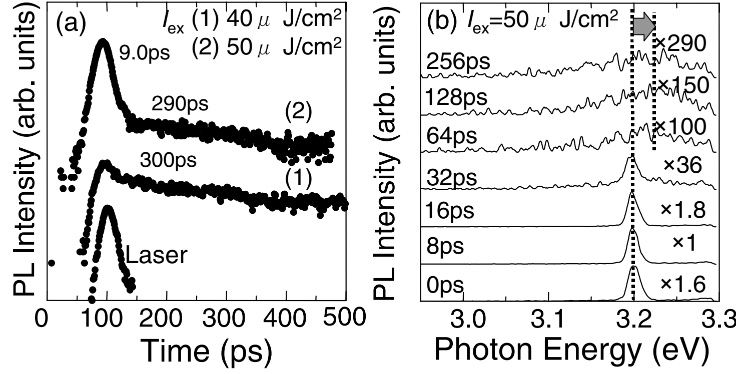

Figure 11. (a) PL decay spectra of the near-UV LD taken from the resonator under just below (40 μJ cm^{-2}) and above (50 μJ cm^{-2}) the lasing threshold. (b) TRPL spectra of the near-UV LD under $I_{ex} = 50$ μJ cm^{-2}.

and c. The decay spectra just below ((1) $I_{ex} = 40$ μJ cm^{-2}) and above ((2) $I_{ex} = 50$ μJ cm^{-2}) the lasing threshold were taken at RT for sample a as shown in figure 11(a). If the I_{ex} value was below the threshold, the decay curve of (1) was expressed with single exponential decay with lifetime of 300 ps. However, the fast decay component as small as 9 ps, originating from the radiative lifetime of stimulated emission, appeared in the spectrum (2). Figure 11(b) shows TRPL spectra as a function of time after pulsed photo-excitation under $I_{ex} = 50$ μJ cm^{-2}. The lasing peak is located at about 3.2 eV just after excitation; however the broadening of spectra was observed after $t = 32$ ps, because of the change of emission mode, namely from stimulated to spontaneous emission. The same measurements have also been performed for sample b as shown in figure 12. The decay time of SE was estimated to be 10 ps. SPE appeared on the low energy side of SE bands after $t \simeq 50$ ps. Figure 13 shows integrated PL intensity for each emission band under various excitation energy densities in three samples. For sample a, the SE band at about 3.2 eV grows super-linearly with increasing I_{ex} values above 50 μJ cm^{-2}. However, for other samples, SE bands peaking at 2.95–2.96 eV (for sample b) and at 2.82–2.85 eV (for sample c) tend to saturate above about 100 μJ cm^{-2}, and a new SE peak appears at about 3.1 eV that is located on the low energy side of E_{ex1hh} SPE bands by about 60–70 meV.

Dynamical behaviour of dense carriers generated by photo-pumping was characterized by measuring the temporal spectra of the differential absorption coefficient as a function of time after pulsed excitation [44]. In the P&P spectroscopy, the transmission spectrum of the probe beam detected in the presence of the pump beam ($T + \Delta T$) is compared to the spectrum without pump beam (T), giving the frequency (ω)-dependent ΔT (ω, I_{ex}, t_d) of the sample for different intensities of the pump (I_{ex}) and for different time delays after the pulsed pumping (t_d). The photo-induced change of optical density [ΔOD(ω, I_{ex}, t_d)] is expressed by the following equation:

$$\Delta \mathrm{OD} = \log\left(\frac{T}{T + \Delta T}\right) = \Delta\alpha d \times 0.434 \tag{2}$$

where $\Delta\alpha(\omega, I_{ex}, t_d)$ is the photo-induced change of absorption coefficient and d is the thickness of absorbing layer. In the normal case, the photo-bleaching ($\alpha + \Delta\alpha < \alpha$) is observed because of the state-filling of photo-induced carrier, and $\alpha + \Delta\alpha$ becomes negative, giving rise to optical gain if the population inversion is achieved. Figure 14(a) shows the variation of differential optical density spectra as a function of time after pumping at 370 nm under $I_{ex} = 200$ μJ cm^{-2} in sample a ($In_{0.1}Ga_{0.9}N$ QW, near-UV LD). The OD spectrum is depicted

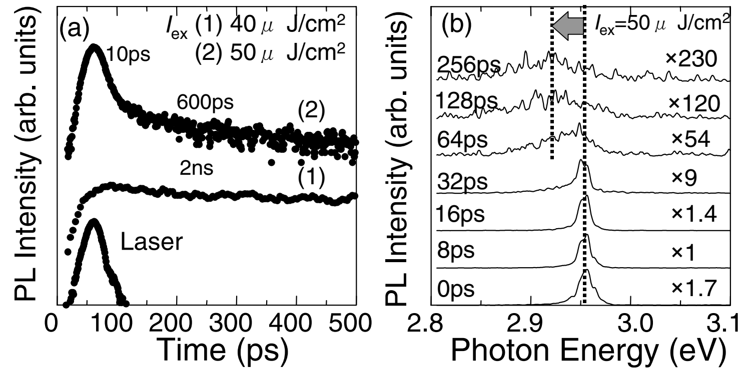

Figure 12. (a) PL decay spectra of the violet–blue LD taken from the resonator under just below (40 μJ cm^{-2}) and above (50 μJ cm^{-2}) the lasing threshold. (b) TRPL spectra of the violet–blue LD under $I_{ex} = 50$ μJ cm^{-2}.

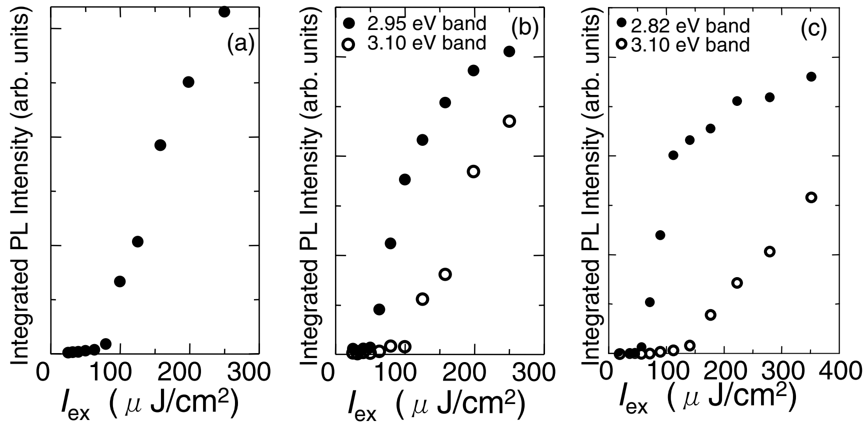

Figure 13. Integrated PL intensity for each emission bands as a function of excitation energy density taken for (a) near-UV LD, (b) violet–blue LD and (c) blue LD.

as a reference. PL spectra of both SE ($I_{ex} = 200$ μJ cm^{-2}) and SPE ($I_{ex} = 100$ nJ cm^{-2}) taken from the surface are also inserted in the figure. The sheet carrier density is roughly estimated to be 1.9×10^{13} cm^{-2} under $I_{ex} = 200$ μJ cm^{-2}. As shown in figure 14(b), at the initial stage of excitation ($t = -500$ fs–0 fs), the bleaching of photo-absorption was observed in the vicinity of the pumping energy. However, the negative peak of ΔOD rapidly reached the level of E_{ex1hh} at a timescale less than 1 ps. The red-shift of E_{ex1hh} was observed with increasing time (13 meV at $t = 200$ ps) probably because the screening of the piezo-electric field is reduced with decreasing carrier density. Optical gain was generated on the low-energy side of the negative peak due to the effect of bandgap renormalization. The data analysis has shown that a maximum optical gain as large as about 8000 cm^{-1} is reached at $t = 1$ ps [44].

Dynamics of dense carriers was also assessed for samples b (violet–blue LD) and c (blue LD) as shown in figure 15. The tail of differential absorption began to grow toward the bottom of localized levels just after the bleaching at E_{ex1hh} was completed. The timescale for reaching the bottom was about 2 ps for sample b, and about 5 ps for sample c. Therefore, it was found that

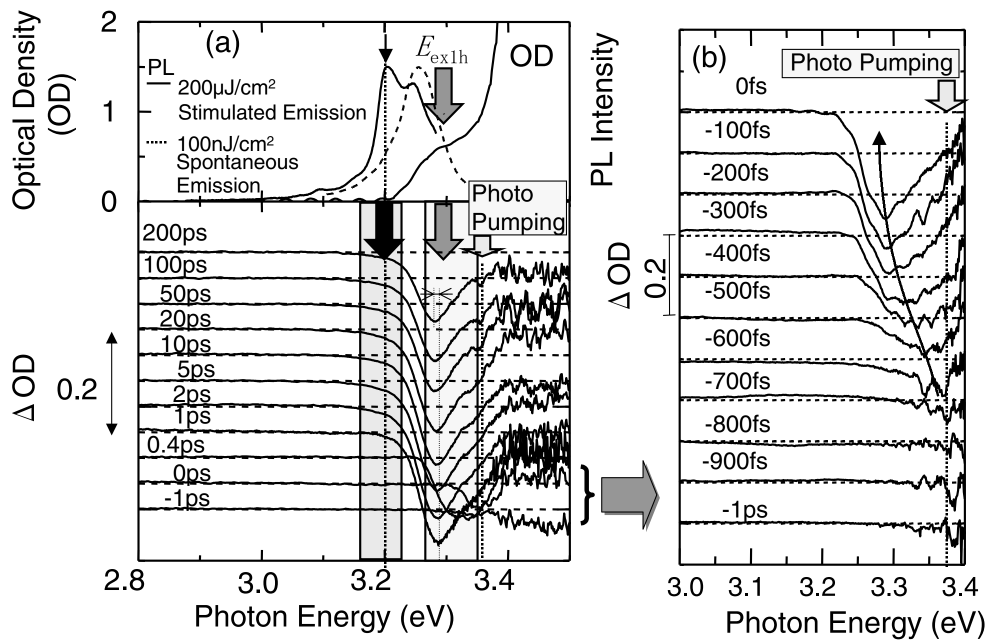

Figure 14. Differential optical density spectra in the time scale (a) from −1 to 200 ps and (b) −1 ps to 0 ps under $I_{ex} = 200$ μJ cm^{-2} taken at the near-UV LD. The OD spectrum taken under low photo-excitation energy density, as well as SE and SPE spectra, are depicted in the figure.

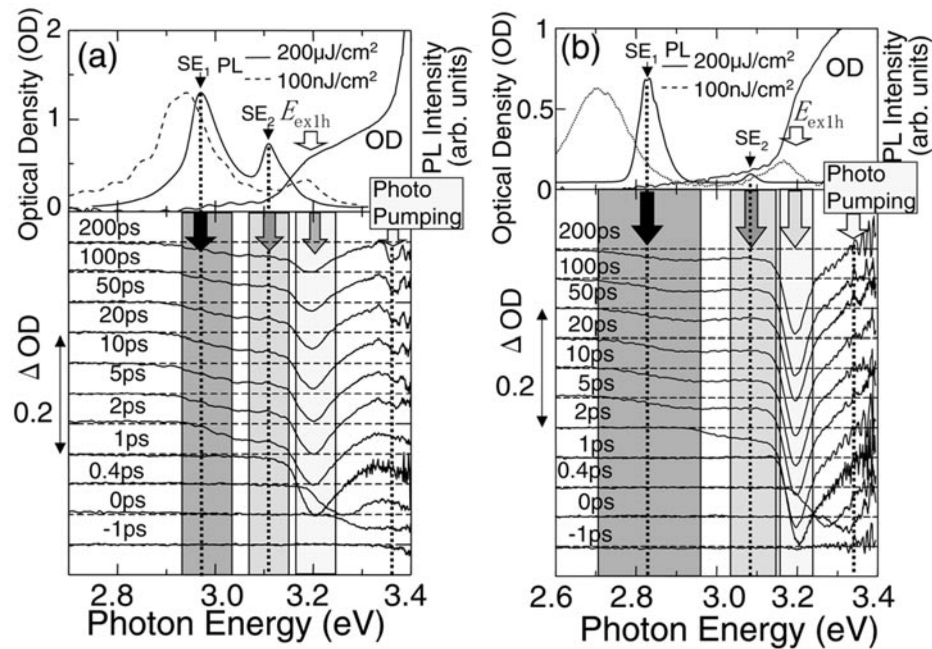

Figure 15. Differential optical density spectra under $I_{ex} = 200$ μJ cm^{-2} taken for (a) the violet–blue LD, and (b) the blue LD. OD spectrum taken under low photo-excitation energy density, as well as SE and SPE spectra, are depicted in the figure.

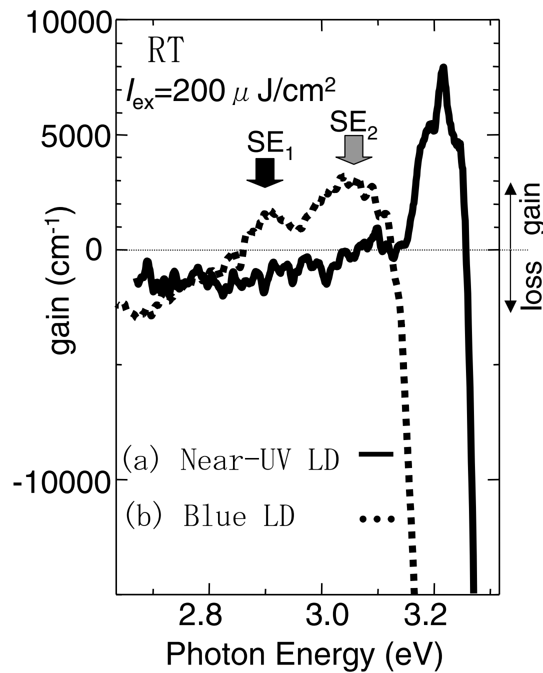

Figure 16. Maximum optical gain spectra in transient spectroscopy under $I_{ex} = 200\ \mu$J cm^{-2} taken for (a) the near-UV LD and (b) the blue LD.

photo-generated carriers and/or excitons efficiently transfer to deeply localized levels without the effect of a phonon bottleneck observed in other QD systems.

Figure 16 shows maximum optical gain spectra in transient spectroscopy in sample a (near-UV LD) and in sample c (blue LD) at RT. For sample a, optical gain appears at 3.2 eV when $I_{ex} > 50\ \mu$J cm^{-2}. Almost no gain saturation is observed up to $I_{ex} = 200\ \mu$J cm^{-2}. However, for sample c, optical gain appears at 2.82 eV when $I_{ex} > 60\ \mu$J cm^{-2}, and gradually makes a blue-shift with I_{ex} reaching at 2.85 eV for $I_{ex} = 200\ \mu$J cm^{-2}. Such gain bands saturate at about 1500 cm^{-1}, and new gain bands grows at about 3.1 eV when $I_{ex} > 100\ \mu$J cm^{-2}.

6. Conclusions

The dynamical behaviour based on localization radiative and nonradiative recombination processes of excitons has been studied in the $In_xGa_{1-x}N$-based LEDs and LDs, by employing the TRPL and the P&P spectroscopy. The addition of small amount of In to the GaN active layer resulted in the suppression of nonradiative recombination centres. It was found that excitons were weakly localized mainly due to the small fluctuation of alloy compositions if the In alloy composition was less than about 10%. The depth of exciton localization grew with increasing In compositions, and the self-formation of deep localization centres was observed in the sample with $x > 20\%$. The zero-dimensional feature of excitons was observed in such a highly localized system. The saturation was observed for the optical gain contributed from such localized states.

Acknowledgment

The authors are grateful for the financial support of a Grant-in-Aid for Scientific Research from the Ministry of Education, Science, Sports and Culture. A part of this work was performed using the facility at the Venture Business Laboratory in Kyoto University (KU-VBL).

References

[1] For a review, see for example, Monemar B, Bergman J P, Dalfors J, Pozina G, Sernelius B E, Holts P O, Amano H and Akasaki I 1999 *MRS Internet J. Nitride Semicond. Res.* **4** 16
[2] Chichibu S, Azuhata T, Sota T and Nakamura S 1996 *Appl. Phys. Lett.* **69** 4188–90
[3] Narukawa Y, Kawakami Y, Funato M, Fujita Sz, Fujita Sg and Nakamura S 1997 *Appl. Phys. Lett.* **70** 981–3
[4] Narukawa Y, Kawakami Y, Fujita Sz, Fujita Sg and Nakamura S 1997 *Phys. Rev.* B **55** R1938–41
[5] Takeuchi T, Wetzel C, Yamaguchi S, Sakai H, Amano H, Akasaki I, Kaneko Y, Nakagawa S, Yamaoka Y and Yamada N 1998 *Appl. Phys. Lett.* **73** 1691–3
[6] Cho Y H, Song J J, Keller S, Minsky M S, Hu E, Mishra U K and DenBaars S P 1998 *Appl. Phys. Lett.* **73** 1128–30
[7] Eliseev P G, Perlin P, Lee J and Osinski M 1997 *Appl. Phys. Lett.* **71** 561–9
[8] Wang T, Sakai H, Bai J, Shirahama T, Lachab M, Sakai S and Eliseev P 2000 *Appl. Phys. Lett.* **76** 1737–9
[9] Lefebvre, Allègre J, Gil B, Kavokine A, Mathieu H, Kim W, Salvador A, Botchkarev A and Morkoç H 1998 *Phys. Rev.* B **57** R9447–50
[10] Narukawa Y, Kawakami Y, Fujita Sg and Nakamura S 1999 *Phys. Rev.* B **59** 10 283–8
[11] Kawakami Y, Narukawa Y, Omae K, Fujita Sg and Nakamura S 2000 *Phys. Status Solidi* a **178** 331–6
[12] Satake A, Masumoto Y, Miyajima T, Asatsuma T, Nakamura F and Ikeda M 1998 *Phys. Rev.* B **57** R2041–4
[13] Schmidt T J, Cho Y H, Gainer G H, Song J J, Keller S, Mishra U K and DenBaars S P 1998 *Appl. Phys. Lett.* **73** 560–2
[14] Chichibu S, Wada K and Nakamura S 1997 *Appl. Phys. Lett.* **71** 2346–8
[15] Zhang X, Rich D H, Kobayashi J T, Kobayashi N P and Dapkus P D 1998 *Appl. Phys. Lett.* **73** 1430–2
[16] Vertikov A, Kuball M, Nurmikko A V, Chen Y and Wang S Y 1998 *Appl. Phys. Lett.* **72** 2645–57
[17] Kaneta A, Izumi T, Okamoto K, Kawakami Y, Fujita Sg, Narita Y, Inoue T and Mukai T 2001 *Japan. J. Appl. Phys.* **40** 110–11
[18] Koukitsu A, Takahashi N, Taki T and Seki H 1996 *Japan. J. Appl. Phys.* **35** L673
[19] Ho I-h and Stringfellow G B 1996 *Appl. Phys. Lett.* **69** 2701
[20] Kisielowski C, Weber Z L and Nakamura S 1997 *Japan. J. Appl. Phys.* **36** 6932–6
[21] Shapiro N, Perlin P, Kisielowski C, Mattos L, Yang J and Weber E 2000 *MRS Internet J. Nitride Semicond. Res.* **5** 1
[22] O'Donnel K P, Martin R W and Middleton P G 1999 *Phys. Rev. Lett.* **82** 237–40
[23] Yang H C, Kuo P E, Lin T Y, Chen Y F, Chen K H, Chen L C and Chyi J I 2000 *Appl. Phys. Lett.* **76** 3712–14
[24] Yamaguchi E and Junnarkar M R 1998 *J. Cryst. Growth* **189/190** 570–4
[25] Bellaiche L, Mattila T, Wang L W, Wei S H and Zunger A 1999 *Appl. Phys. Lett.* **74** 1842–4
[26] Kudo H, Tanabe T, Ishibashi H, Zheng R, Yamada Y and Taguchi T 2000 *Phys. Status Solidi* a **180** 27–31
[27] Nakamura S, Senoh M, Iwasa N, Nagahama S, Yamada T and Mukai T 1995 *Japan. J. Appl. Phys.* **34** L1332–5
[28] Nakamura S, Senoh M, Iwasa N, Nagahama S, Yamada T and Mukai T 1998 *Japan. J. Appl. Phys.* **37** L479–81
[29] Nakamura S, Senoh M, Nagahama S, Iwasa N, Yamada T, Matsushita T, Kiyoku H and Sugimoto Y 1996 *Japan. J. Appl. Phys.* **35** L74–6
[30] Nagahama S, Iwasa N, Senoh M, Matsushita T, Sugimoto Y, Kiyuko H, Kozaki T, Sano M, Matsumura H, Umemoto H, Chocho K and Mukai T 2000 *Japan. J. Appl. Phys.* **39** L647–50
[31] Mukai T and Nakamura S 1999 *Japan. J. Appl. Phys.* **38** 5735–9
[32] Mukai T, Takekawa K and Nakamura S 1998 *Japan. J. Appl. Phys.* **37** L839–41
[33] Nakamura S, Senoh M, Nagahama S, Iwasa N, Matsushita T and Mukai T 2000 *Appl. Phys. Lett.* **76** 22–4
[34] Cho Y, Schmidt T, Bidnyk S, Gainer G, Song J, Keller S, Mishra U and DenBaars S 2000 *Phys. Rev.* B **61** 7571–88
[35] Im J, Kollmer H, Off J, Sohmer A, Scholz F and Hangleiter A 1998 *Phys. Rev.* B **57** R9435–8
[36] Narukawa Y 2000 Emission mechanism in quantum well structures composed of GaN-based semiconductors *PhD Thesis* Kyoto University, pp 104–11
[37] Mukai T, Yamada M and Nakamura S 1998 *Japan. J. Appl. Phys.* **37** L1358–61
[38] Miller R, Kleinman D, Nordland W Jr and Gossard A 1980 *Phys. Rev.* B **22** 863–71

[39] Feldman J, Peter G, Göbel E, Dawson P, Moore K, Foxon C and Elliot R 1987 *Phys. Rev. Lett.* **59** 2337–40
[40] Gotoh H, Ando H, Takagahara T, Kamada H, Chavez-Pirson A and Temmyo J 1997 *Japan. J. Appl. Phys.* **36** 4204–8
[41] Narukawa Y, Saijou S, Kawakami Y, Fujita Sg, Mukai T and Nakamura S 1999 *Appl. Phys. Lett.* **74** 558–60
[42] Okamoto K, Ko H C, Kawakami Y and Fujita Sg 2000 *J. Cryst. Growth* **214/215** 639–45
[43] Izumi T, Narukawa Y, Okamoto K, Kawakami Y, Fujita Sg and Nakamura S 2000 *J. Lumin.* **87–89** 1196–8
[44] Kawakami Y, Narukawa Y, Omae K, Nakamura S and Fujita Sg 2000 *Appl. Phys. Lett.* **77** 2151–3